water

MDPI

Article

Experimental Study on the Influence of Barrier Structures on Water Renewal Capacity in Slow-Flow Water Bodies

Longyang Pan [1], Xingguo Yang [1,2], Yeong-bin Yang [1,3], Hongwei Zhou [1,2,*], Rui Jiang [4], Junyi Cai [1], Niannian Li [1] and Jiamei Wang [1]

[1] College of Water Resource and Hydropower, Sichuan University, Chengdu 610065, China
[2] State Key Laboratory of Hydraulics and Mountain River Engineering, College of Water Resource and Hydropower, Sichuan University, Chengdu 610065, China
[3] School of Civil Engineering, Chongqing University, Chongqing 400045, China
[4] China Three Gorges Project Development Co., Ltd., Chengdu 610041, China
* Correspondence: hw.zhou@scu.edu.cn

Abstract: Artificial islands and viewing pavilions can act as barriers in slow-flow water bodies such as lakes and can be used together with water diversion projects to improve the water quality. In this study, based on the particle image velocimetry system, we carried out flume experiments to study the influence of the location and shape of barriers on the purification capacity of a slow-flow water body. We analyzed the velocity composition based on the information entropy H and the vector distributions, average velocity and water exchange rate η. The results reveal that the hydrodynamic characteristics are significantly optimized by barrier structures. η doubles if the barrier structure is reasonably designed, and it is positively correlated with the average velocity. In all cases, the highest η is recorded for a barrier shaped as a rectangular column and increases with the interaction area between the flow and structure. The water purification capacity and flow velocity gradually increase with increasing flow rate. The influence of the relative distance l between the inlet and the structure on η is non-monotonic. To achieve a higher η, the l for the rectangular column, triangular prism, and semi-cylinder should be 0.2–0.3, 0.2–0.3, and 0.3–0.55, respectively. The deflection angles and the ratio of lateral velocity to streamwise velocity of the deflection mainstream decrease with increasing l. H for the rectangular column is higher than that for other shapes. The results are of guiding significance for the layout of barrier structures and for the optimization of water landscapes in practical applications.

Keywords: slow-flow water body; barrier structure; water exchange rate; average velocity; velocity composition

Citation: Pan, L.; Yang, X.; Yang, Y.-b.; Zhou, H.; Jiang, R.; Cai, J.; Li, N.; Wang, J. Experimental Study on the Influence of Barrier Structures on Water Renewal Capacity in Slow-Flow Water Bodies. *Water* **2022**, *14*, 3757. https://doi.org/10.3390/w14223757

Academic Editor: Giuseppe Pezzinga

Received: 17 September 2022
Accepted: 15 November 2022
Published: 18 November 2022

1. Introduction

A slow-flow water body is a closed or semi-closed water body with low fluidity, a low exchange rate, poor reoxygenation ability and weak self-purification ability, which has not yet been clearly defined [1,2]. According to the flow velocity in which the growth of submerged vegetation is not significantly inhibited in relevant studies [3–5], it can be preliminarily considered that the flow velocity of slow-flow water is generally 0–0.35 m/s. Slow-flow water bodies, such as landscape wetlands, reservoirs, and artificial lakes, are increasingly common with the construction and development of hydraulic ecosystems. Owing to the influence of point or non-point source pollution and insufficient supplies of fresh water sources, a large number of slow-flow water bodies have been significantly polluted and their water quality has degraded [6–9]. Taking measures to protect the water quality of slow-flow water is of great significance for water ecosystem restoration, ecological construction and landscape optimization.

The water exchange process refers to the process of water exchange and integration between slow-flow water and external water bodies, and between different water bodies

within slow-flow water [10]. It is a key factor that affects the water quality [11], which can be evaluated by water age, renewal time, etc. [12,13]. The water exchange process can affect the chlorophyll content, suspended sediment distribution and water turbidity [14–16]. The water exchange process is also susceptible to the wind field, tide, topography and other factors [17–20]. The complex hydrodynamic process is of great significance to alleviate and control lake eutrophication [21]. Therefore, it is urgent to study the water exchange process of slow-flow water bodies and the measures that need to be taken to promote the water exchange process, so as to optimize the water quality and hydrodynamic characteristics of these bodies of water.

The promotion of water exchange is regarded as a healthy and efficient method to alleviate eutrophication and improve water ecology [22–24]. A water diversion project is a common method that is used to solve water quality deterioration and alleviate water pollution [25–27], which has been widely proved to have complex effects on water ecosystems [28–30]. Water diversion projects can significantly reduce the water age of the water body (especially in the center of the water body) [17], shorten the residence time [31] and reduce the comprehensive restoration time [32]. It can increase the surface area and restore the degraded water systems [33], and the water circulation system constructed by the water diversion projects can effectively improve the current speeds, reduce the proportion of stagnation areas, and increase the velocity in low-velocity zones [34,35]. The diversion water has an obvious influence on the flow velocity near the intake [36]. The efficiency of water diversion is easily affected by wind conditions, water transfer routes, water transfer schemes, ecological water demand and other factors [37,38]. Li et al. [39] proposed that 98.4% of the lake areas could be covered under the appropriate water transfer routes and schemes. Research on the water diversion projects of Taihu Lake showed that the dual-source diversion method has better advantages than the single-source diversion method under normal circumstances [40], and the sluice and pump diversion in artificial lakes could improve the water quality in the whole wading area [41]. Due to the complex influence of water diversion projects on the water exchange process in lakes [42], blind water diversion may not be able to fully improve the water quality [43,44], so it is very important to study the influence of water diversion projects on the hydrodynamic characteristics and water quality of slow-flow water bodies.

Recently, the landscape design of slow-flow water bodies often involves piers, pillars and artificial islands of various shapes [45–47]. Relevant research shows that the average velocity, turbulence intensity and Reynolds shear stresses around the complex piers with pile caps are lower than those around the simple piers [48], and the turbulence intensity increases with pier size in the presence of ice cover [49]. Flow field analysis shows that in the area upstream of the pier, the streamwise component of velocity becomes positive for which the universal log-law turns out to be valid [50]. The construction of artificial islands affects the flow field around the islands [51,52]. Liu et al. [53] proposed that a reasonable arrangement of artificial islands could enhance channel exchange, which could improve water exchange capacity to a certain extent. Relevant research mainly focuses on the flow field and velocity profile around the structures [54,55], while there are few studies on the water exchange process under the influence of the barrier structures in the slow-flow water.

The combination of water diversion projects and structure design represents one of the most important ways to improve the ecological environment of slow-flow water bodies. It is of great application value to study the influence of structures on hydrodynamic characteristics and water exchange efficiency. In this paper, we carried out flume experiments to study the influence of the location and shape of barrier structures on the renewal capacity of slow-flow water bodies. The data of the two-dimensional flow field of the slow-flow water body influenced by a barrier structure were recorded using a particle image velocimetry (PIV) system. Additionally, based on the principle of information entropy, the changes in the two-dimensional flow field, water exchange rate, average velocity, and velocity of the deflected mainstream center were processed and analyzed. The main purpose of this study is to reveal the following: (1) the influence of structure shape on the two-dimensional flow

field of the water surface and water exchange rate; (2) the response of the two-dimensional flow field and water exchange rate to the adjustment of the location of the barriers. The research results can guide the design and location adjustment of barrier structures to enhance water exchange capacity and promote pollutant removal in slow-flow water bodies under the influence of diversion projects. This study provides a method and technical reference for quantitative comparative analysis and improvement of water exchange capacity.

2. Experimental Methods

2.1. Experimental Facility and Instrumentation

As shown in Figure 1, the generalized physical device consists of a main water flume, a water reservoir and a tail water-collecting tank. Considering that lakes are mainly shallow and wide, the normal physical model will lead to a water depth that is too shallow, so a distorted model was adopted in this study [56,57]. The main flume was modeled on Xinglong Lake in Chengdu City. The length and width of the main water area are approximately 1.7 and 1.2 km, respectively, and the ratio is about 1.4. The main flume was a plexiglass rectangular flume that was 80 cm in length, 60 cm in width, and 10 cm in height, which meets the length and width ratio of Xinglong Lake. The bottom was horizontal to the ground. Inlet and outlet flumes with a width of 5 cm were set on the one side of the flume. The inlet was connected to a reservoir that was 40 cm in length, 40 cm in width, and 60 cm in height through a water inlet chute. Water pipes with an inner diameter of 21 mm were connected to both sides of the reservoir. An inlet valve and a turbine flowmeter were installed. To produce different flow rates, the inlet and outlet valves of the reservoir were adjusted to stabilize the water level at different heights. A baffle was placed at the outlet of the flume to stabilize the water level at 5 cm. The water flowing out of the flume was collected by the water tank and transported to the reservoir by a circulating pump. Taking Xinglong Lake in Chengdu City as the prototype, a series of generalized physical experiments were designed to study the two-dimensional hydrodynamic process under the water diversion projects. The flow characteristics and barrier structure's influence were considered by ignoring the influence of boundary conditions. The influence of wind field was not considered in this experiment. The relationship among the diversion flow rates, artificial structure and hydrodynamic characteristics was mainly studied and revealed.

Surface velocity is an important parameter to describe the characteristics of flow, and is the external embodiment of the internal turbulent structure. As an important hydrological factor, the distribution of surface velocity directly or indirectly controls the diffusion of pollutants and sediment movement [58,59]. It is of great significance to measure and analyze the flow field of the water surface. Therefore, this paper focuses on the two-dimensional hydrodynamic characteristics of the water surface under the combined action of the barrier structures and water diversion projects. The above experimental settings meet the requirements.

Recently, PIV systems are often used to record flow field or wind field. The system uses advanced non-contact flow measurement technology to present the flow field of a water body. By measuring and calculating the displacement of tracer particles in the water body at a known time interval, the fluid velocity and flow field distribution can be determined. Laser irradiation and image acquisition processes can take measurements without interfering in the whole process [60–63]. In this study, the two-dimensional flow field of a stable water surface was measured using PIV, and the application is shown in Figure 1. The camera was fixed and was perpendicular to the water surface. The laser emitted by the sheet light source overlapped with the water surface to illuminate the particles for shooting. PIV was always measured at the water surface 5 cm from the flume bottom. The tracer particles were hollow glass beads with a particle size of 8–12 μm and a median particle size of 10 μm, which can effectively reflect the motion characteristics of water. The capture frequency was set at 5 Hz, that is, five sets of data were collected every second and the original data were stored. Based on the data, the time-averaged two-

dimensional flow field of the water surface was obtained for the stable water. After being processed by the PIV system, the flow field data were further calculated and analyzed.

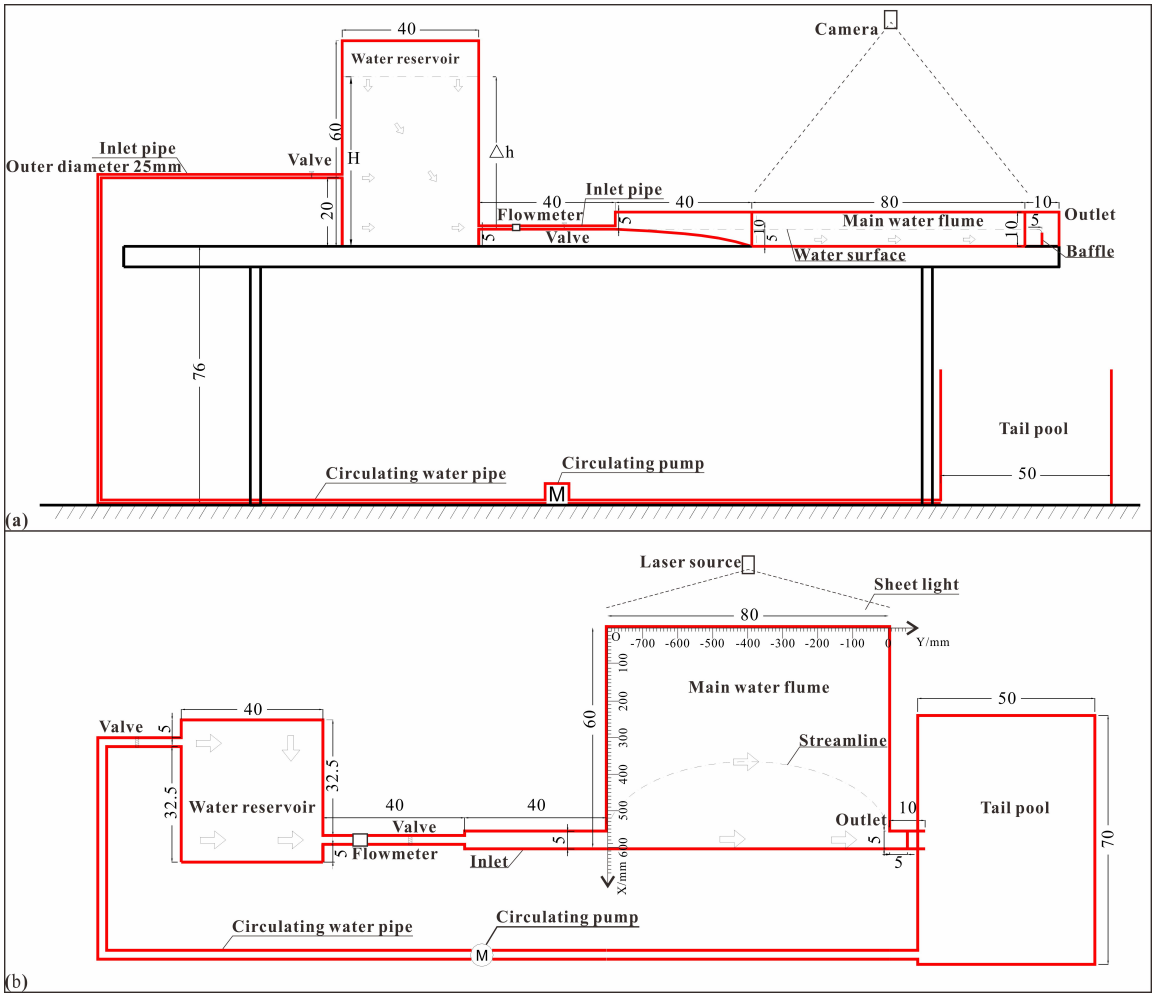

Figure 1. Experimental installation: (**a**) side view of the flume; (**b**) top view of the flume (point O is the axis origin, and the unit of the numbers in the figure is cm, except for those already indicated).

2.2. Experimental Similarity Rule and Data Processing

Considering the experiment was carried out with clean water, ignoring the viscosity effect may cause some errors, but it has little impact on the experimental results and the qualitative law. The experiments and analysis are carried out while respecting the criterion of Froude similarity (gravity similarity), and the geometric parameters and kinematic parameters of the prototype and model in the system mainly follow the relationship shown in Formula (1).

$$\lambda_{L,v,t,Q} = \frac{L, v, t, Q_{prot}}{L, v, t, Q_{mod}},\ \lambda_v = \lambda_L^{1/2},\ \lambda_t = \lambda_L^{1/2},\ \lambda_Q = \lambda_L^{5/2} \quad (1)$$

The longitudinal length of the flume, Y = 80 cm, was chosen to normalize the flume lengths. The surface velocity of the flow field was normalized by the average stream velocity at the upstream end of the slow-flow water. The calculation method and values are shown in Formula (2).

$$l = \frac{L}{Y},\ v_{ni} = \frac{v_i}{v_{in}},\ v_{in} = \frac{Q_{min}}{A} = \frac{3.7\ \text{L/min}}{25\ \text{cm}^2} = 0.025\ \text{m/s} \quad (2)$$

where L is the distance between the water inlet and the structure centroid (cm); v_{ni} is the dimensionless velocity; v_i is the surface velocity of each point in the flow field (m/s).

The evaluation quantities of the hydrodynamic characteristics include the water renewal time, retention time, water age, water exchange rate, half exchange time and other parameters [11,64–67]. With a shorter water renewal time, retention time, and higher water exchange rate and average velocity, the water purification capacity is stronger. Generally, the conservative substance with an initial concentration of 1 is placed in the lake, and the percentage of the total substance transported outside the area compared to the total initial substance percentage after a period of time is the water exchange rate [68,69]. In contrast, Zhang et al. [70] analyzed the change in a stagnant water area with a velocity lower than the set velocity. Based on this, this study uses the water exchange rate based on critical velocity and two-dimensional surface average velocity to describe the water purification capacity and hydrodynamic characteristics. In addition, the surface velocity information entropy is used to analyze the velocity composition of the water surface. The determination of critical velocity is related to the hydrodynamic exchange and water nutrient status [71,72]. According to the ratio of the average velocity in Xinglong Lake to the critical velocity of algae growth in the lake, which is about 1.2 [73,74], the maximum dimensionless average velocity with no structures in this study is 0.24–0.285, and the critical velocity is determined to be about 0.2 by dividing 0.24 by 1.2. The calculation methods of the water exchange rate and the average velocity are as follows:

$$\eta = \frac{S - S_0}{S} \tag{3}$$

$$\overline{v} = \frac{\sum v_{ni}}{\sum i} \tag{4}$$

where η is the water exchange rate (dimensionless), S is the total surface area of the slow-flow water (cm^2), and S_0 is the total area of the stagnant water area (cm^2), $\overline{v}$ is the average velocity (dimensionless); v_{ni} is the normalized velocity at each point in the flume. Water with a surface velocity lower than 0.2 cannot be purified effectively, which is called the stagnant water area. Two conditions are randomly selected to show the distribution of the stagnant water area, and S_0 is shown in Figure 2. Note that the white area is due to the fact that the vector arrow, whose speed is below the critical speed, is not displayed.

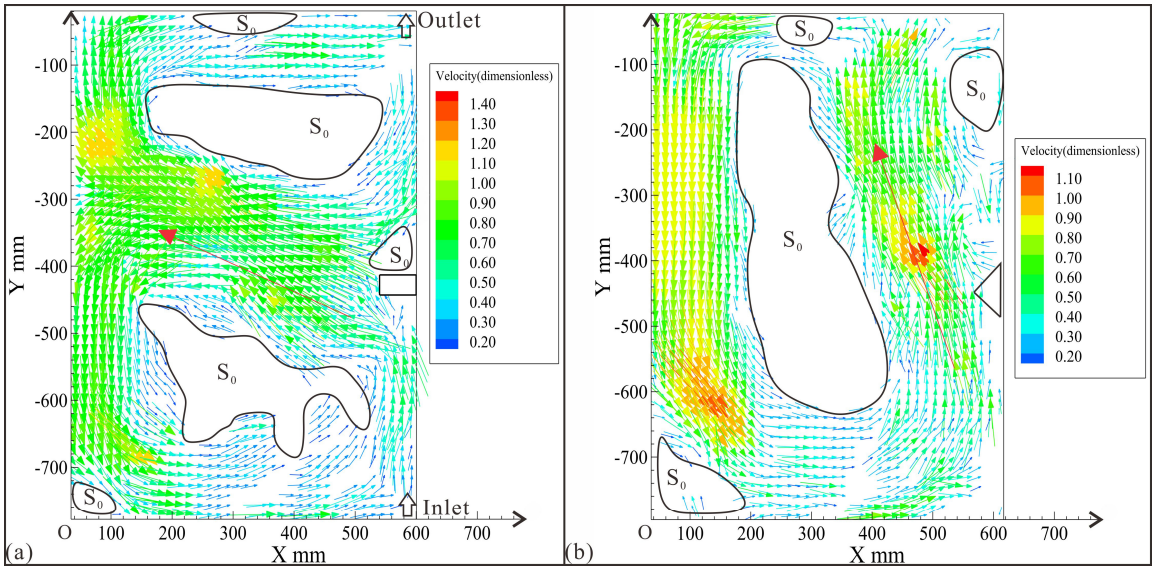

Figure 2. Distribution of the stagnant water area: (**a**) rectangular column, Q = 6.8 L/min, l = 0.44; (**b**) triangular prism, Q = 6.8 L/min, l = 0.44.

In this study, the velocity composition of the flow field under various conditions is discussed and analyzed based on the principle of information entropy. Information entropy was first proposed by Shannon in 1984, and is used to measure the amount of information, stability and uncertainty of a system and to characterize the evolution characteristics. The lower the entropy value is, the higher the order degree of the system is [75–77]. Entropy H is given according to the work of Shannon et al., as shown in Formula (5) [78,79].

$$H = -\sum P_i log_2 P_i \quad (5)$$

where P_i is the probability of a symbol showing up in a given system of symbols, and the use of the logarithm base two corresponds to the expression of information entropy in terms of bits. In entropy calculations, the dimensionless velocities of each point in the two-dimensional flow field processed by the PIV system are obtained. The maximum dimensionless velocity in all conditions is 1.64. The velocity values of the flow field are divided into the following nine intervals: v_{n1} (0–0.164), v_{n2} (0.164–0.328), v_{n3} (0.328–0.492), v_{n4} (0.492–0.656), v_{n5} (0.656–0.820), v_{n6} (0.820–0.984), v_{n7} (0.984–1.148), v_{n8} (1.148–1.312), v_{n9} (1.312–1.64), and the corresponding P_1, P_2, P_3, P_4, P_5, P_6, P_7, P_8, P_9 values, respectively For the selected two-dimensional system, the total grid number N of the flow field and N_i (i = 1–9) that corresponds to each interval v_{ni} are calculated, respectively. Then, $P_i = N_i/N$ is calculated. Finally, the information entropy of the velocity composition under different conditions is calculated according to Formula (5).

2.3. Experimental Conditions

Considering the shapes of common islands and artificial structures in lakes, three generalized shapes were considered for the barrier structure, namely a triangular prism, semi-cylinder, and rectangular column. The shapes and sizes of the three structures and their locations in the flume are shown in Figure 3. The structures of the three shapes were placed along the side wall of the flume and on the line between the inlet and outlet. In addition, only one shape was placed at a time in the location set by the experiment. There was no sequence. All of the structures were made from organic glass. According to the water inlet width of 5 cm, the structural dimensions were designed as follows: the front edge width of the rectangular column was 6 cm, the right-angle side length of the triangular prism was 6 cm, and the diameter of the semi-cylinder was 6 cm.

The experimental conditions are shown in Table 1. The location of the structure was defined by the distance L between the inlet and the structure centroid, which is 15, 25, 35, 45, and 55 cm, respectively. The normalized relative distance l is 0.19, 0.31, 0.44, 0.56, and 0.69, respectively. The inflow flow rate Q of the flume was adjusted by the water depth of the reservoir, and the corresponding flow rates Q were 3.7, 4.5, 5.3, 6.0, and 6.8 L/min for the water depths of 24, 33, 39, 48, and 58 cm, respectively. Experiments were carried out without structures as references for comparative analysis.

Table 1. Experimental conditions (C for semi-cylinder, R for rectangular column; T for triangular prism).

Experiment Conditions	Q (L/min)	l	Structural Shape	Experiment Conditions	Q (L/min)	l	Structural Shape
R1-0-0	3.7	—	—	R3-3-2	6.0	0.56	T
R1-1-1		0.19	R	R3-3-3			C
R1-1-2			T	R3-4-1			R
R1-1-3			C	R3-4-2			T
R1-2-1		0.31	R	R3-4-3			C
R1-2-2			T	R3-5-1	6.8	0.69	R
R1-2-3			C	R3-5-2			T

Table 1. *Cont.*

Experiment Conditions	*Q* (L/min)	*l*	Structural Shape	Experiment Conditions	*Q* (L/min)	*l*	Structural Shape
R1-3-1	3.7	0.44	R	R3-5-3	6.0	0.69	C
R1-3-2			T	R4-0-0		—	—
R1-3-3			C	R4-1-1		0.19	R
R1-4-1		0.56	R	R4-1-2			T
R1-4-2			T	R4-1-3			C
R1-4-3			C	R4-2-1		0.31	R
R1-5-1		0.69	R	R4-2-2			T
R1-5-2			T	R4-2-3			C
R1-5-3			C	R4-3-1		0.44	R
R2-0-0	4.5	—	—	R4-3-2			T
R2-1-1		0.19	R	R4-3-3			C
R2-1-2			T	R4-4-1		0.56	R
R2-1-3			C	R4-4-2			T
R2-2-1		0.31	R	R4-4-3			C
R2-2-2			T	R4-5-1		0.69	R
R2-2-3			C	R4-5-2			T
R2-3-1		0.44	R	R4-5-3			C
R2-3-2			T	R5-0-0	6.8	—	—
R2-3-3			C	R5-1-1		0.19	R
R2-4-1		0.56	R	R5-1-2			T
R2-4-2			T	R5-1-3			C
R2-4-3			C	R5-2-1		0.31	R
R2-5-1		0.69	R	R5-2-2			T
R2-5-2			T	R5-2-3			C
R2-5-3			C	R5-3-1		0.44	R
R3-0-0	5.3	—	—	R5-3-2			T
R3-1-1		0.19	R	R5-3-3			C
R3-1-2			T	R5-4-1		0.56	R
R3-1-3			C	R5-4-2			T
R3-2-1		0.31	R	R5-4-3			C
R3-2-2			T	R5-5-1		0.69	R
R3-2-3			C	R5-5-2			T
R3-3-1		0.44	R	R5-5-3			C

Notes: 'Ra-b-c' is the abbreviation of Run. The first number 'a' after R represents different flow rates, and 1~5 corresponds to 3.7~6.8 L/min, respectively. The second number 'b' represents the relative distance *l*, and 1~5 corresponds to 0.19~0.69, respectively. The third number 'c' represents the patch shapes, and 1~3 corresponds to the rectangular column, triangular prism and semi-cylinder. 'Ra-0-0′ indicates that no vegetation patch is set in water.

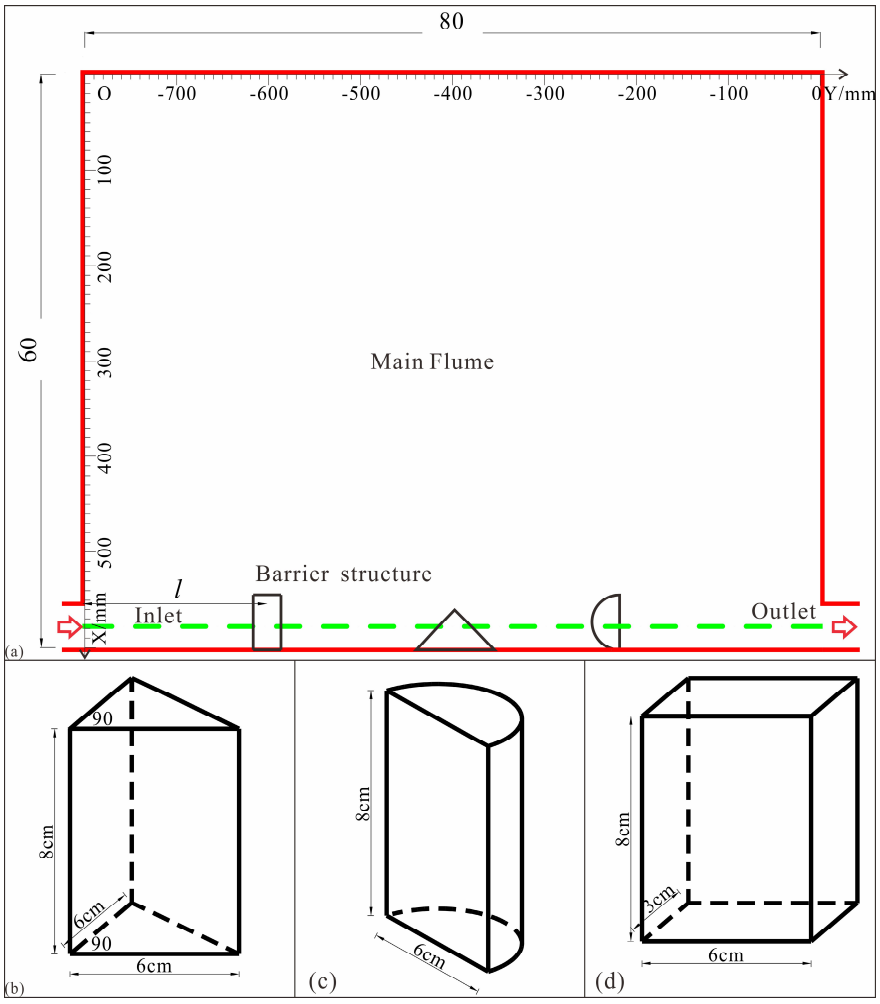

Figure 3. Schematic diagram of barrier structures in water body: (**a**) structure location; (**b**) triangular prism; (**c**) semi-cylinder; (**d**) rectangular column.

3. Experimental Results

3.1. Flow Field Distribution

The direct effect of the barrier structures on the slow-flow water body under the water diversion projects is shown in the change in the flow field, including the change in the velocity magnitude and vector distribution, and the circulation formation and distribution. This paper mainly introduces the influence of the flow rate Q, structure shape and location on the flow field. The interaction intensity and location between the mainstream and structure change with the structure location l and inlet flow rate Q.

Figure 4 shows the two-dimensional vector distributions of the water surface for the rectangular column and when Q = 3.7, 6.8 L/min. For the water with no structures, the flow field is mainly composed of the obvious mainstream, which flows straight between the inlet and outlet and the circulation is reported close to the flume wall. For the high and low flow rates, the mainstream velocities reach about 0.556–0.962 and 0.649–0.977, and the circulation velocities are about 0.463–0.898 and 0.342–0.570, respectively. The circulation velocity increases significantly with increasing Q, but the velocity in the center area is only about 0.034, indicating poor dynamic conditions. For Q = 3.7 L/min and l = 0.19, lateral flow is formed around the structures without obvious circulation. The lateral distance is about one half of the flume width, and the mainstream velocity is about 0.642–1.069. For l = 0.31, two obvious circulations are formed and the deflection mainstream velocity is about 0.748–1.112. For larger l (greater than 0.31), the lateral distance of the deflection mainstream decreases gradually. A complete circulation is formed in the flume and the

area increases gradually. For l = 0.56 or 0.69, the lateral velocity of the deflection flow is approximately 0. Corresponding to l = 0.44, 0.56 and 0.69, the flow velocities before the addition of the structures are 0.335–1.155, 0.371–1.055, and 0.364–0.920, respectively, and flow velocities after deflection are 0.584–1.190, 0.527–1.048, and 0.435–0.877, respectively. The deflection flow velocity decreases with increasing l. The mainstream velocity can be improved by placing the structures in the water, and the high-velocity area is mainly distributed in the circulation or deflection flow. For high flow rates (Q = 6.8 L/min) and when l = 0.19, 0.31 and 0.44, two obvious circulations between the structures and the inlet or outlet are formed. The mainstream velocities can reach about 0.670–1.247, 0.620–1.262, and 0.670–1.247. The longitudinal velocities are relatively small. The proportion of high-velocity areas will increase with the increasing Q. For l = 0.56 and 0.69, the lateral velocities of the deflection flow decrease to 0.485–0.905 and 0.143–0.784, respectively. The lateral distance decreases and the distance for l = 0.69 is the smallest. A single circulation that covers a large area is formed in the flume. The circulation velocities can reach about 0.820–1.247 and 0.684–1.005. For a large l, circulation close to the flow field with no structures is formed at different flow rates, but the velocity of the circulation center is generally 0.093–0.235, which is not conductive to water purification. The deflection effect between the flow and structure is expressed in the deflection angle and the ratio of the lateral to longitudinal velocity. For Q = 6.8 L/min, the deflection angle is approximately 90° for l = 0.19 or 0.31, and approximately 60° for l = 0.56 or 0.69.

Figures 5 and 6 show the two-dimensional vector distribution of the water surface for the triangular prism and semi-cylinder and when Q = 3.7, 6.8 L/min. When placing the triangular prism into the water, for Q = 3.7 L/min and l = 0.19, the mainstream interacts with the structure without diffusion. A circulation is formed between the structure and the outlet, and obvious flow around the structure can be found with velocities of about 0.627–0.969. For l = 0.31, 0.44, 0.56, and 0.69, the flow forms a large-area circulation after the deflection of the structures, and the deflection angles near the structure are about 45°. The lateral velocity of the deflection flow is approximately 0, and the longitudinal movement is still dominant. The deflection flow velocities can reach about 0.513–0.912, 0.463–0.920, 0.492–0.912, and 0.442–0.763. It can be found that the velocities after deflection are significantly higher for a small l, and the velocities of the circulation center are about 0.053–0.135, with lower water purification efficiency. For Q = 6.8 L/min, the width of the deflection flow noticeably increases. For l = 0.19, 0.31, and 0.44, the deflection flow forms a large-area circulation and a small-area circulation near the outlet. The mainstream velocities can reach 0.734–1.105, 0.627–1.148, and 0.670–1.190. Moreover, the ratio of the lateral velocity to longitudinal velocity is larger, that is, 0.217–0.97, 0.0015–0.647, and 0.0047–0.448. For l = 0.56 and 0.69, the vector distribution is similar to that at low flow rates, and the mainstream velocities can reach about 0.663–1.076 and 0.620–1.540. The lateral velocity compared to the deflection velocity is almost 0. When the semi-cylinder is placed in the water, a large-area circulation forms at low flow rates. With increasing l, the mainstream velocities can reach 0.456–0.934, 0.385–0.948, 0.421–0.905, 0.356–0.905, and 0.385–0.884. For a large l (0.56, 0.69), the lateral flow is not obvious after deflection, mainly due to the decrease in the interaction intensity caused by the mainstream diffusion and the smooth surface of the semi-cylinder, and the lateral distance of the flow is obviously reduced. The exchange capacity at the back of the structure is poor. The overall distribution of the flow field at high flow rates is similar to that at low flow rates. With the increase in l, the mainstream velocities can be about 0.556–1.119, 0.642–1.176, 0.520–1.198, 0.627–1.140, and 0.599–1.233, respectively. The lateral distance decreases, and the flow field distributions tend to be stable.

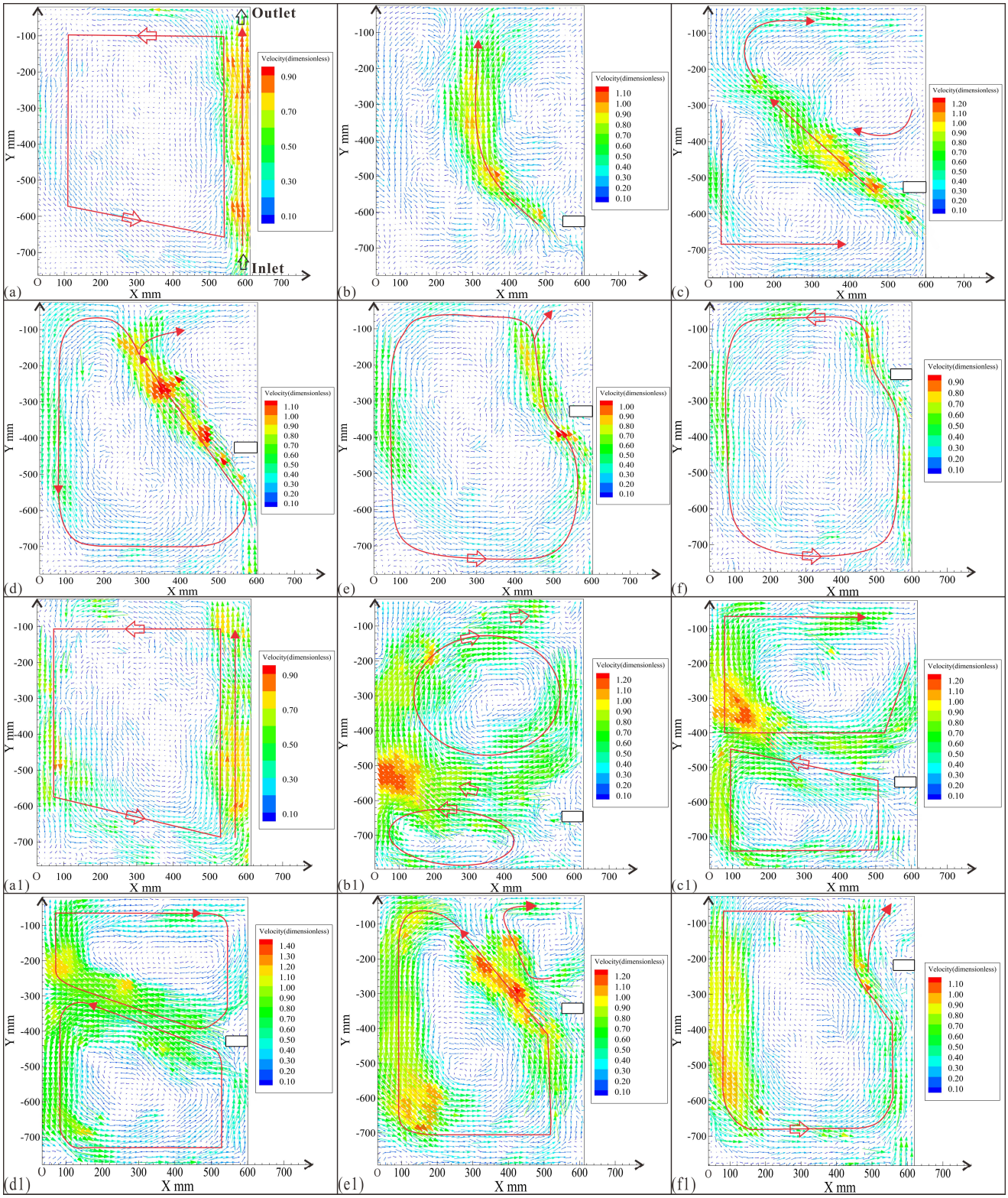

Figure 4. Vector distribution of the flow field under the influence of the rectangular column for Q = 3.7 L/min and 6.8 L/min, respectively: (**a**–**f**) for 3.7 L/min; (**a1**–**f1**) for 6.8 L/min. Vector distribution (**a**,**a1**) for no structure; (**b**,**b1**) for l = 0.19; (**c**,**c1**) for l = 0.31; (**d**,**d1**) for l = 0.44; (**e**,**e1**) for l = 0.56; (**f**,**f1**) for l = 0.69.

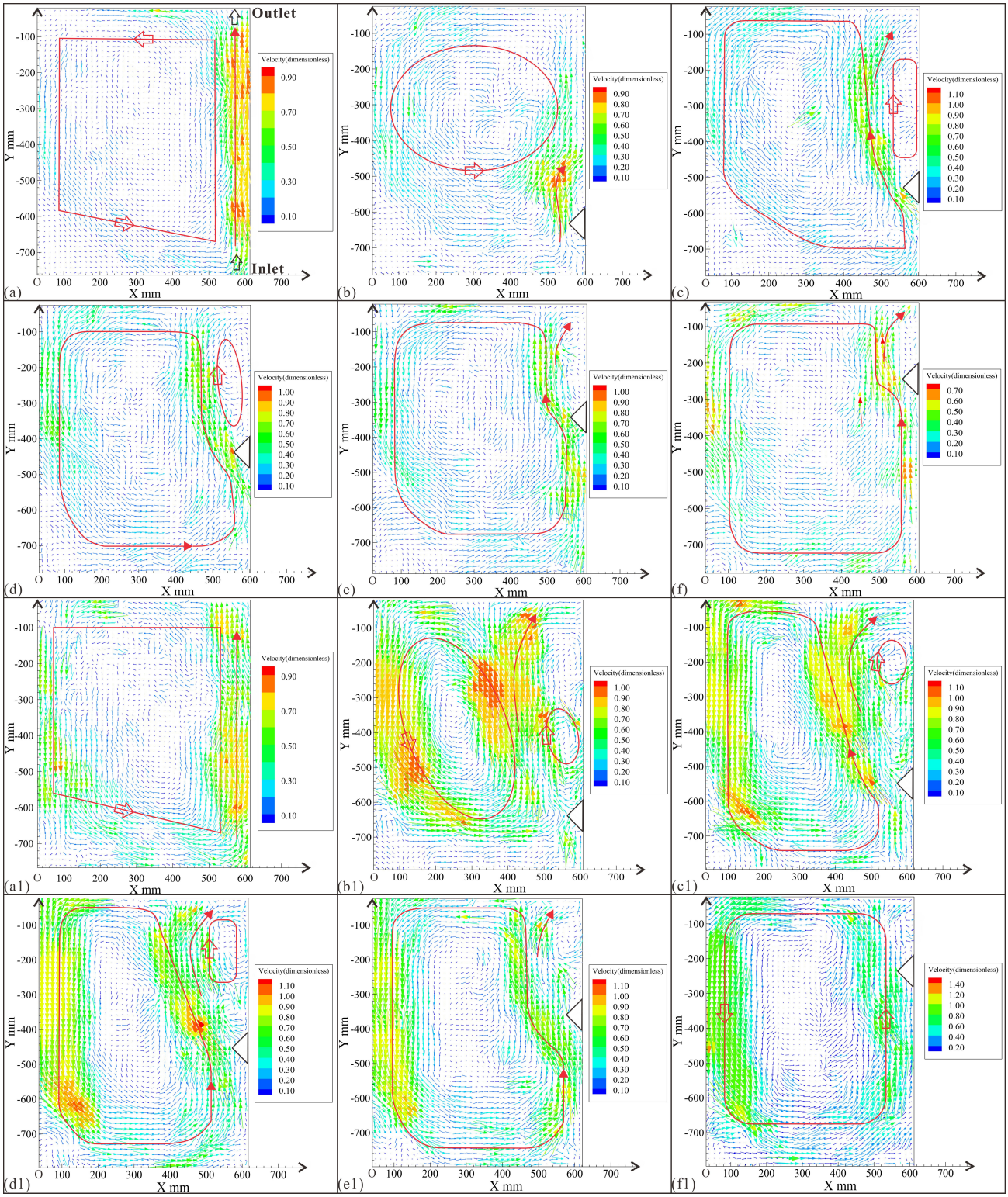

Figure 5. Vector distribution of the flow field under the influence of the triangular prism for Q = 3.7 L/min and 6.8 L/min, respectively: (**a**–**f**) for 3.7 L/min; (**a1**–**f1**) for 6.8 L/min. Vector distribution (**a**,**a1**) for no structure; (**b**,**b1**) for l = 0.19; (**c**,**c1**) for l = 0.31; (**d**,**d1**) for l = 0.44; (**e**,**e1**) for l = 0.56; (**f**,**f1**) for l = 0.69.

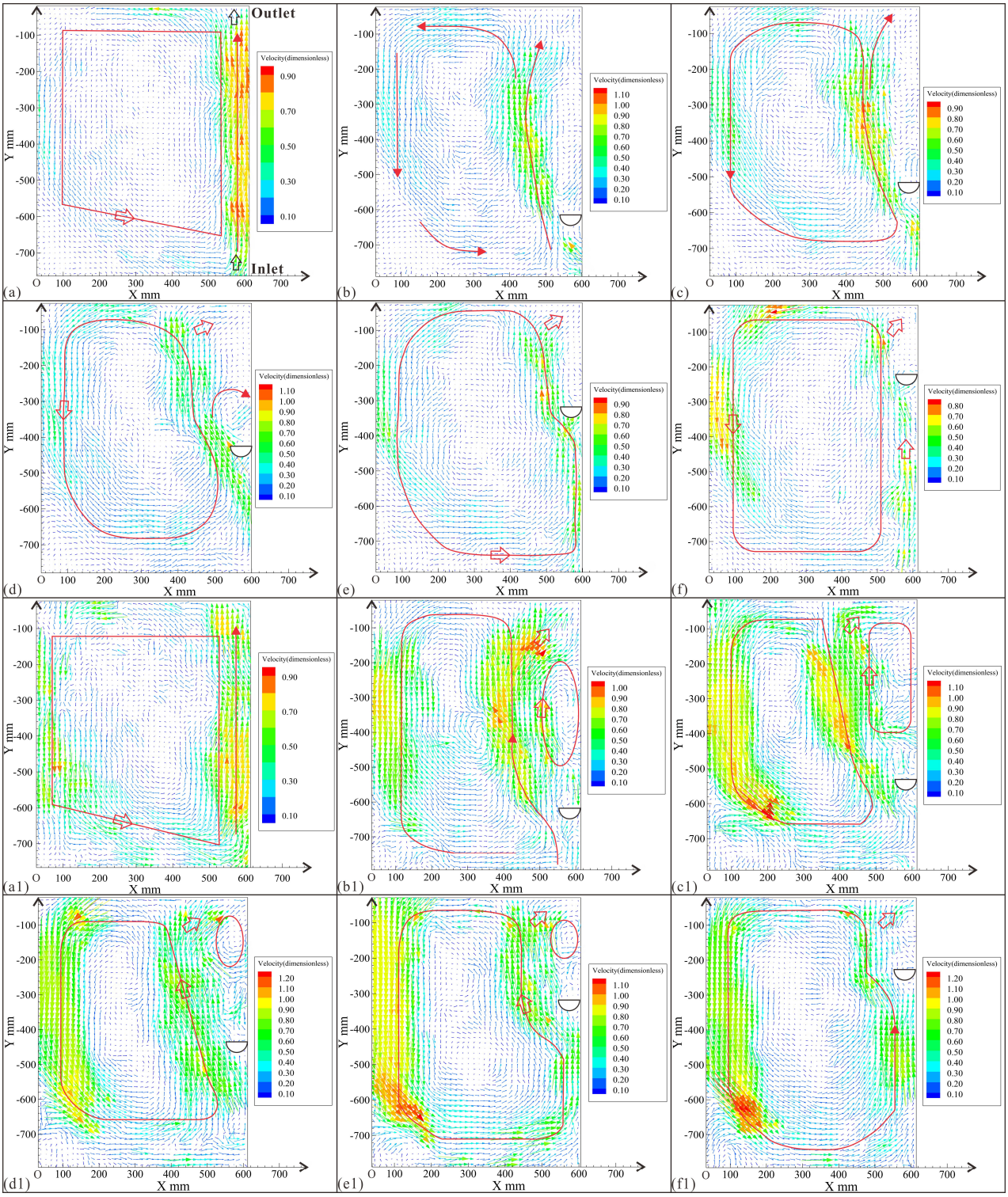

Figure 6. Vector distribution of the flow field under the influence of the semi-cylinder for Q = 3.7 L/min and 6.8 L/min, respectively: (**a**–**f**) for 3.7 L/min; (**a1**–**f1**) for 6.8 L/min. Vector distribution (**a**,**a1**) for no structure; (**b**,**b1**) for l = 0.19; (**c**,**c1**) for l = 0.31; (**d**,**d1**) for l = 0.44; (**e**,**e1**) for l = 0.56; (**f**,**f1**) for l = 0.69.

3.2. Velocity Variation

To process the deflection mainstream to optimize the flow field, the velocity variation along the deflection mainstream under the influence of the flume wall and the surrounding water was studied. The line location was selected, as shown in Figure 7. For Q = 6.8 L/min

and l = 0.31 and 0.56, the variations in the deflection mainstream velocity that correspond to the three structures are shown in Figure 8, where a is the straight-line distance from each point of the deflected mainstream to the structure. For l = 0.31, the velocity along the path increases rapidly to the maximum values of 1.026 (a = 3 cm) and 1.005 (a = 4 cm) for the triangular prism and semi-cylinder, respectively. Subsequently, the velocity fluctuates along the path, starts to decrease at 33 and 37.5 cm, and finally approaches zero. For the rectangular column, the flow velocity starts to fluctuate around 0.299, as the strong interaction between the flow and structure causes the flow to break and disperse. The velocity starts to increase to its maximum value of 0.763 from 25 cm, which is due to the convergence of high-intensity circulation at this point and the flow velocity starts to drop to 0 at 52 cm. The velocity for the rectangular column is lower than that for the other two structures. For l = 0.56, the velocities for the three structures fluctuate along the path and show a downward trend as a whole. After deflection, the initial velocity varies in the following order: rectangular column > triangular prism > semi-cylinder. The maximum values of the velocity along the path are 1.297, 0.920, and 0.627, corresponding to a = 7, 0, and 0 cm, respectively. The velocity along the mainstream for the rectangular column after deflection is higher than that for the other two shapes.

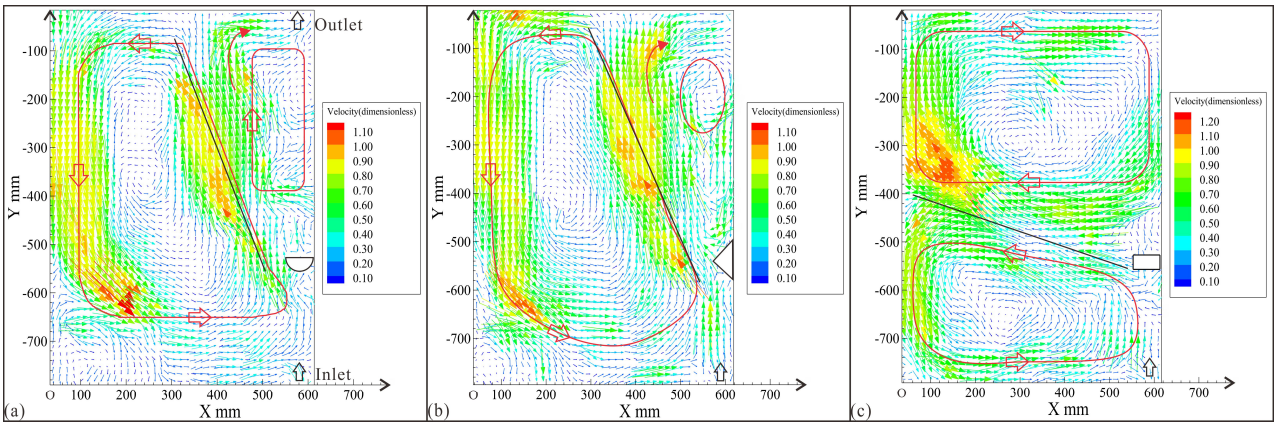

Figure 7. Straight line of the mainstream center (black line): (**a**) semi-cylinder, Q = 6.8 L/min, l = 0.31; (**b**) triangular prism, Q = 6.8 L/min, l = 0.31; (**c**) rectangular column, Q = 6.8 L/min, l = 0.31.

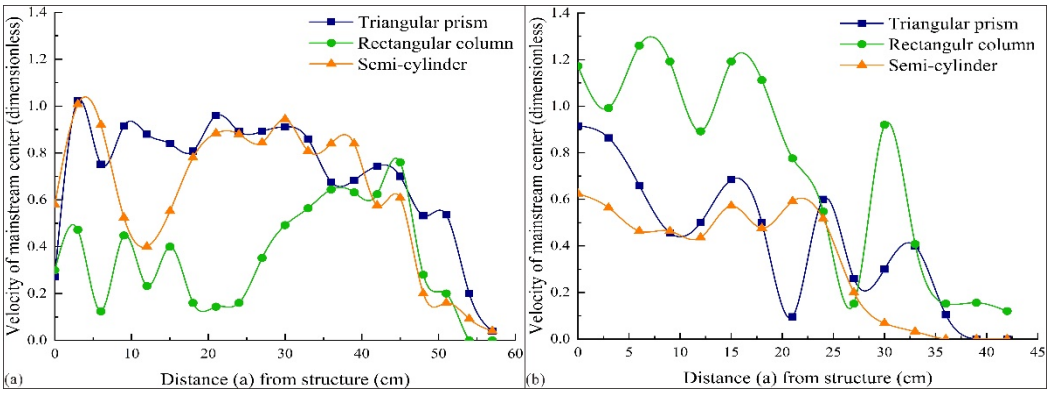

Figure 8. Variation in the velocity along the deflection mainstream center: (**a**) l = 0.31; (**b**) l = 0.56 (a is the straight-line distance from each point of the deflected mainstream to the structure).

3.3. Water Exchange Rate and Average Velocity

Figure 9 shows the change in the water renewal capacity for the triangular prism with different locations under each flow rate. For a small Q (3.7 L/min), with increasing l, the water exchange rate η first increases to its highest value (η = 36%), is stable when l = 0.31–0.56 and then decreases. For Q = 4.5 L/min, η first increases and then decreases,

with the maximum value of 59.86% (l = 0.31). When Q is greater than 4.5 L/min, η decreases with increasing l, but for Q = 6.0, 6.8 L/min, η increases for a larger l. The minimum value of η for Q = 5.3, 6.0, and 6.8 L/min is 42.52%, 54%, and 55%, which corresponds to l = 0.69, 0.56, and 0.56, respectively. For the same l, with increasing Q, the overall average velocity increases continuously. The average velocity for a small distance and high flow rate (l = 0.19, Q = 6.8 L/min) is the largest, and η under this condition is the highest (η = 68.49%). The overall average velocity for a small distance and low flow rate (l = 0.19, Q = 3.7 L/min) is the smallest, and that for a low flow rate varies slightly with l and it is maintained below 0.2.

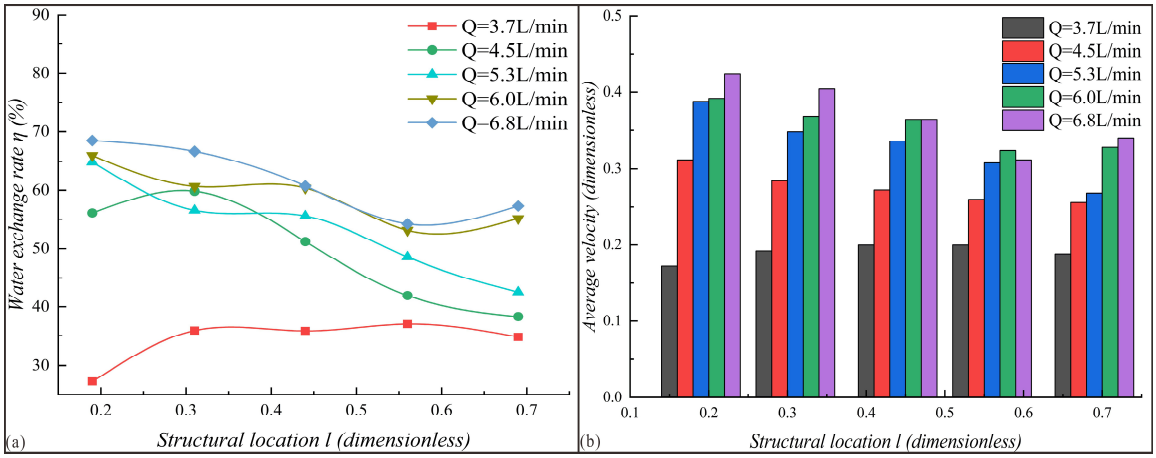

Figure 9. Calculation results for the triangular prism: (**a**) water exchange rate; (**b**) average velocity.

Figure 10 shows the change in the water renewal capacity for the semi-cylinder with different locations under each flow rate. The water exchange rate η and average velocity both first increase and then decrease with increasing l for different flow rates. For Q = 3.7 L/min, η is the smallest and reaches its maximum value when l = 0.44 (η = 37.61%). For Q = 5.3 L/min, the variation trend of η is similar to that for Q = 4.5 L/min, and it reaches its maximum value when l = 0.31 (η = 57.15%). When Q is greater than 5.3 L/min, η is lower than 60% when Q = 6.0, 6.8 L/min. The maximum average velocity (0.364) and η (58.96%) is achieved for Q = 6.8 L/min and l = 0.31. For l = 0.19 and Q > 5.3 L/min, the average velocity varies slightly, which indicates that the structure strongly blocks the flow and Q has no evident influence on the average velocity. The velocity under this condition is maintained at 0.32. The average velocity increases with increasing flow rate.

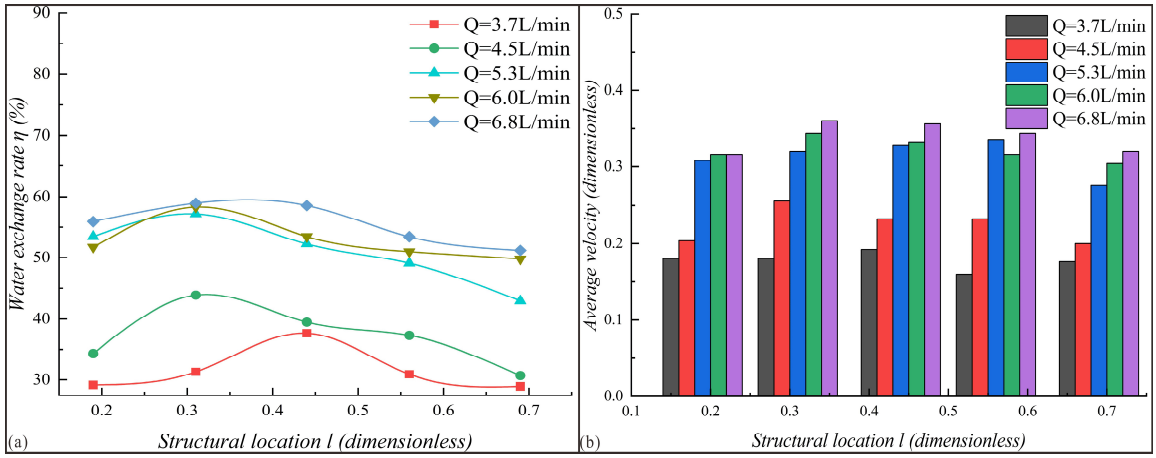

Figure 10. Calculation results for the semi-cylinder: (**a**) water exchange rate; (**b**) average velocity.

Figure 11 shows the change in the water renewal capacity for the rectangular column with different locations under each flow rate. When Q is 3.7, 4.5 L/min, η first increases and then decreases with increasing l, and reaches its maximum value of 45.30% and 52.60% at l = 0.31, respectively. When Q is greater than 5.3 L/min, η decreases with increasing l. The maximum η is 76.21% when Q = 6.8 L/min and l = 0.19. η for the rectangular column at the same location increases with increasing Q. The optimal structure location to achieve maximum η is different for different Q. The average velocity is the highest (0.456) for Q = 6.8 L/min and l = 0.19. For the same l, the changing trend of the average velocity with increasing Q is different.

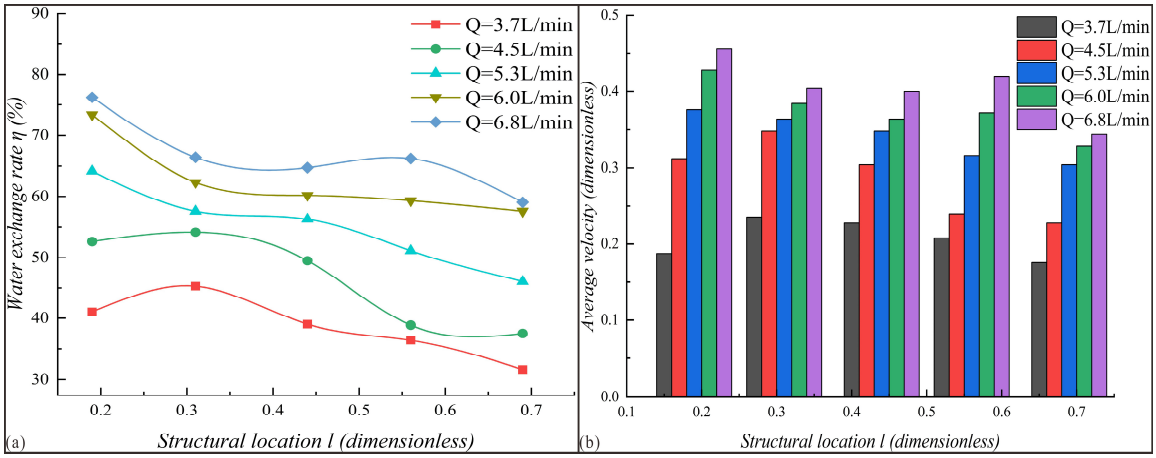

Figure 11. Calculation results for the rectangular column: (**a**) water exchange rate; (**b**) average velocity.

3.4. Information Entropy Analysis

In order to comprehensively analyze the velocity composition and the proportion of each velocity interval and the changing rule with experimental conditions, the calculation results of the information entropy of the velocity composition under the influence of the triangular prism, semi-cylinder and rectangular column are shown in Figure 12. The larger the information entropy H is, the smaller the difference among the different intervals in the flow field system is. Otherwise, it means that the system will be dominated by a certain velocity interval. For the triangular prism and when Q = 6.8, 6.0 L/min, with the increase in l, H decreases first and then increases and the following values were reported: 2.582, 2.584, 2.483, 2.346, 2.426 and 2.545, 2.457, 2.479, 2.285; 2.356. When the structure is located in the middle of the flume wall, the proportion of the velocity interval of 0–0.328 increases significantly. The proportion of the low-velocity (0–0.328) interval for other l decreases, but that for the other intervals increases significantly, and the velocity composition tends to be more uniform. For Q = 5.3 and 4.5 L/min, H gradually decreases with the increase in l. For a large l, the low-velocity interval (0–0.164) proportion gradually increases, demonstrating obvious dominance in the flow field. For Q = 3.7 L/min, H increases first and then decreases with increasing l. For the semi-cylinder, H increases first and then decreases with the increase in l, reaching 1.423–1.682 (3.7), 2.193–2.429 (4.5), 2.129–2.376 (5.3), 2.204–2.392 (6.0) and 2.282–2.491 (6.8). For l = 0.3–0.6, the proportion of the intervals 0–0.328 and 0.656–0.820 is reduced, and that of the high-velocity interval (0.820–1.148) increases. For the rectangular column, it can be found that the increase in l (less than 0.5) at low flow rates (3.7 and 4.5 L/min) will reduce the proportion of the low-velocity interval (0–0.328), and significantly improve that of the higher-velocity interval (0.492–0.820).

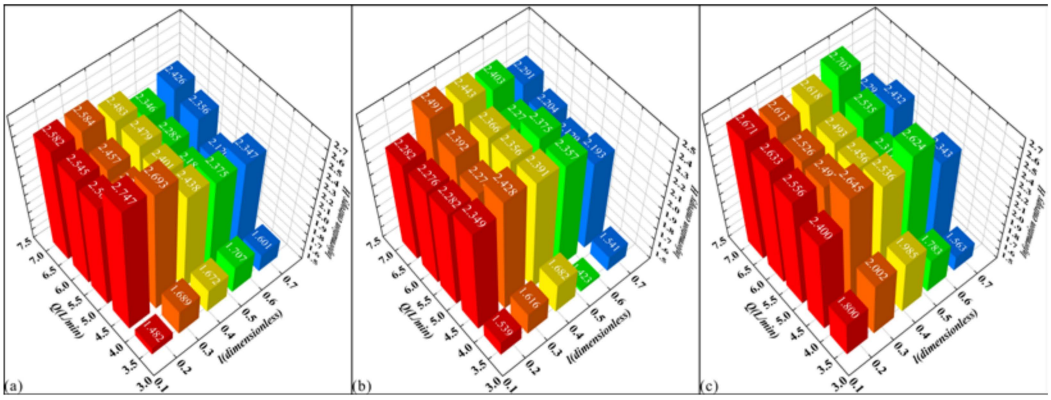

Figure 12. Calculation results of the information entropy of the two-dimensional flow field: (**a**) triangular prism; (**b**) semi-cylinder; (**c**) rectangular column.

On the whole, the flow rate Q has a significant influence on the information entropy H, and when $Q > 3.7$ L/min, H increases greatly, indicating that the increase in flow rates can reduce the proportion of the low-velocity interval and proportion difference among each interval. At high flow rates, the flow velocity composition is more uniform and the overall velocity increases. H for the rectangular column is larger under various conditions, indicating that the rectangular column plays a more obvious role in the adjustment of the velocity composition, while H for the semi-cylinder is relatively smaller. When H corresponds to 3.7–6.8 L/min with no structures, the following values were reported: 1.348, 1.867, 1.563, 1.873, and 2.003.

4. Discussion

Three parameters were varied for the experiment series. The influence of the structure location, structure shape and flow rate on the water exchange rate, average velocity and velocity information entropy is considered. Compared with various annular flow fields formed in lakes with no structures [14,17,21,34], and by considering the poor flow velocity in the center of lakes [27], placing structures in the water will obviously optimize the flow path and the velocity composition, which can be observed from the calculation results of the average velocity and information entropy. The water exchange rate η for water with no structures is 21.61–44.43%, and this parameter increases significantly after the structures are placed in the water.

The structure location determines the location where the inflow and the structures interact, and the deflection location and angle of the mainstream, thus changing the exchange rate. With the increase in l, circulation gradually appears and changes from complex circulations to a single large-scale circulation. The deflection effect of the structure is weakened, the deflection angle is reduced, and the lateral velocity and the ratio of the lateral velocity to longitudinal velocity of the deflection mainstream are gradually decreased. The collision location between deflection flow and the flume wall shifts. The influence of l on the exchange rate is non-monotonic. In order to achieve a higher η, l for the rectangular column, semi-cylinder, and triangular prism should be 0.2–0.3, 0.3–0.55, and 0.2–0.3, respectively. When the structure is close to the inlet, the flow interacts with the structure without obvious diffusion (this can be found from the decrease in the deflection mainstream velocity, as l increases from 0.19–0.44). The island in the rivers can reduce the stream width to improve the flow [46], and the effect is better for a smaller l in this paper. For a smaller l, the turbulence intensity at the back of the structure is higher, because the blocking effect of the structure results in part of the kinetic energy of the inflow water being converted into potential energy, and part of the kinetic energy enhances the extrusion velocity of the flow around the structure, which leads to turbulence at the back of the structure, enhancing the mixing effect [45,54].

Different structure shapes result in different interaction areas and deflection directions, changing the deflection angle, mainstream velocity, and the water exchange rate. Existing studies have shown that pier diameter, shapes and other factors influence the flow field significantly [47,80,81]. The deflection angle that corresponds to the triangular prism and semi-cylinder is approximate and relatively small, generally about 30–45°, while that for the rectangular column is larger, approximately 90° for small l and decreases as l increases. The triangular prism can compress and accelerate the flow for small l. At various distances, η for the rectangular column is relatively larger, while that for the semi-cylinder is relatively smaller. This may be because the inclined plane or curved surface of the triangular prism and semi-cylinder produces a stable transition flow when interacting with the flow, and the interaction intensity is weak. The interaction area between the rectangular column and the flow is relatively large, the deflection effect is greater and the optimization effect on the flow field is more obvious (mostly consistent with the calculated results of the information entropy). Owing to the influence of the circulation on both sides of the mainstream and the turbulent mixing of local water, the velocity along the deflection mainstream decreases gradually, with fluctuations. In some cases, the flow velocity decreases significantly before the collision with the flume wall, which may be due to the energy loss caused by the collision between the flow and the flume, forming a low-velocity or stagnant water zone near the wall, blocking the incoming flow and leading to a rapid decline in velocity.

The flow rate Q determines the inlet flow velocity, and the interaction intensity between the flow and barrier structures. For water with no structures and with an increase in Q, both η and the average velocity increase. The residence time will also be shortened [32], and the equilibrium concentration of the water quality index shows a downward trend [36]. For a small Q (3.7 L/min), the interaction is weak, and the correlation between η and structure location is relatively weak. For a large Q, the correlation is significantly enhanced. When the distance is small (l = 0.19), for the rectangular column, the deflection angle is about 45–50° for a small Q (3.7 L/min), while it obviously increases to about 90° after Q increases, indicating that the interaction intensity is significantly enhanced. It should be noted that the excessive diversion flow rates will greatly change the flow field and are not conducive to water ecology [40].

In this paper, water exchange rate η and average velocity are selected as parameters to evaluate the hydrodynamic characteristics, and the information entropy H is calculated to evaluate the variation in velocity composition. We pointed out the calculation results in Figure 13. There is a good correlation between η and average velocity, as R^2 = 0.94. However, the correlation between H and average velocity is relatively weak, as R^2 = 0.68. When H increases, the proportion of each velocity interval becomes more uniform. When H is small, the low-velocity interval (especially 0–0.164 or 0.164–0.328) demonstrates obvious dominance, and the average velocity is relatively small. As H increases, it indicates that the corresponding proportion of other high-velocity intervals increases, and the average velocity should increase. Therefore, the two parameters also present a positive correlation.

We studied the influence of the structure location and shape on the renewal capacity of the slow-flow water body based on the physical experiments. Considering the change in flow rates, the reasonable selection of the location and shape of the structure or artificial island can obviously improve the hydrodynamic characteristics of the lakes or other water bodies, which is of great significance in the optimization of water quality and landscape design. It should be noted that the quantity and location of the inlet and outlet have a significant influence on the water quality [19,22]. In this paper, the inlet and outlet are fixed at the edge of the flume, which may not be the best, as they are restricted by the solid boundary and the friction of the side wall. The flow at the inlet and outlet is stable, and the flow in the flume is mostly constant during the experiments. The flow field was measured under stable conditions in the flume, which can be considered as representative. Next, further study should be carried out according to the structure of the barriers, artificial island design and water boundary conditions.

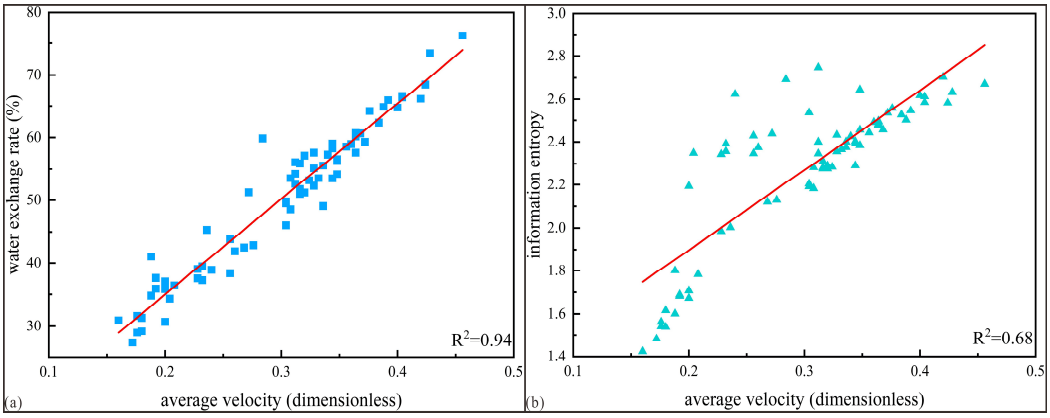

Figure 13. Fitting diagram of three parameters: (**a**) water exchange rate and average velocity; (**b**) information entropy and average velocity.

5. Conclusions

The influence of barrier structure location and shape on the renewal capacity and hydrodynamic characteristics of slow-flow water bodies was studied in laboratory experiments based on the PIV system. The vector distribution, water exchange, average velocity of the flow field, and velocity variation along the deflection mainstream center were obtained by processing the two-dimensional flow field data. The average velocity and water exchange rate η were selected as the measurable quantities, and the information entropy H was calculated to evaluate the velocity composition. The main conclusions are as follows:

1. There is a good positive correlation between η and average velocity (R^2 = 0.94). Compared with η of 21.61–44.43% of water with no structures, placing barrier structures in the water can significantly improve the water exchange rate (up to twice its value). The results are of practical significance for designing and adjusting structures in water to improve water quality.
2. The location parameter l changes the deflection mainstream velocity and direction, and its influence on η is non-monotonic. With the increase in l, circulation gradually appears and the area gradually expands. The deflection angle and the ratio of lateral velocity to streamwise velocity decrease, and the deflection effect of the structure weakens. The flow field for a large l (0.69) is similar to that with no structures. To achieve a higher η by placing structures in the water, the optimal l that corresponds to the triangular prism, rectangular column, and semi-cylinder is 0.2–0.3, 0.2–0.3, and 0.3–0.55, respectively.
3. Structures have different effects on the flow field due to the different interaction surfaces, and the resistance effect of the rectangular column is the strongest. The deflection angles for the triangular prism and semi-cylinder are about 30°–45° at various flow rates, and these will be smaller for a larger l. The deflection angle of the rectangular column can be 90° for a smaller l, and the influence on the flow field is more obvious. In all cases, η for the rectangular column is relatively large, while that for the semi-cylinder is relatively small. A larger interaction area between the flow and structures generally results in a higher η.
4. The flow rate Q is an important factor that affects water renewal capacity, changing the interaction intensity between the flow and structures. The average velocity and η increase with the increase in Q, and the flow rate that corresponds to the maximum η is generally 6.8 L/min.
5. The information entropy H varies positively with the average velocity (R^2 = 0.68). H for the rectangular column is larger, indicating that the rectangular column plays a more obvious role in adjusting the velocity composition, while H for the semi-cylinder is relatively smaller.

Author Contributions: Conceptualization, L.P., X.Y. and H.Z.; Experiment, L.P., R.J., J.C. and N.L.; Data Analysis, L.P. and J.W.; Writing—Original Draft, L.P.; Writing—Review and Editing, X.Y., Y.-b.Y. and J.W.; Project Administration, H.Z. All authors have read and agreed to the published version of the manuscript.

Funding: This research was funded by the Key Technology Research of Urban Slow-Flow Water Body Construction and Protection Program, Feasibility Study on Landscape Upgrading Project of Erlongtan Reservoir Area and Bank in Gao County, and Research and Application Demonstration of Beidou High-Precision Urban Disaster Risk Forecast and Early Warning System (No. 2022YFG0016-LH).

Data Availability Statement: Data in this work are available from the corresponding author upon reasonable request (hw.zhou@scu.edu.cn (Hongwei Zhou)).

Acknowledgments: This work was supported by the Key Technology Research of Urban Slow-Flow Water Body Construction and Protection Program, and Feasibility Study on Landscape Upgrading Project of Erlongtan Reservoir Area and Bank in Gao County. The authors acknowledge the cooperation of all the participants in this study.

Conflicts of Interest: The authors declare no conflict of interest.

References

1. Zhao, N.; Cao, Y.Q.; Huang, L.Y. Repairing Technology and Protection Countermeasures for Slow-Flow Water Bodies Pollution. *S. North Water Transf. Water Sci. Technol.* **2008**, *6*, 101–103. (In Chinese) [CrossRef]
2. Gao, J.; Dang, H.; Liu, L.; Kong, S. Pollution survey and countermeasures of urban slow-flow water body. *Appl. Mech. Mater.* **2012**, *178–181*, 661–665. [CrossRef]
3. Olsen, Y.S.; Fraser, M.W.; Martin, B.C.; Pomeroy, A.; Lowe, R.; Pedersen, O.; Kendrick, G.A. In situ oxygen dynamics in rhizomes of the seagrass Posidonia sinuosa: Impact of light, water column oxygen, current speed and wave velocity. *Mar. Ecol. Prog. Ser.* **2018**, *590*, 67–77. [CrossRef]
4. Peralta, G.; Brun, F.G.; Perez-Llorens, J.L.; Bouma, T.J. Direct effects of current velocity on the growth, morphometry and architecture of seagrasses: A case study on Zostera noltii. *Mar. Ecol. Prog. Ser.* **2006**, *327*, 135–142. [CrossRef]
5. Ke, X.; Li, W. Hormonal correlates of seedling growth of two Vallisneria species growth at different current velocities. *Hydrobiologia* **2006**, *556*, 243–249. [CrossRef]
6. Wu, C.Y.; Chen, W. Indicator system construction and health assessment of wetland ecosystem—Taking Hongze Lake Wetland, China as an example. *Ecol. Indic.* **2020**, *112*, 106164. [CrossRef]
7. Chang, N.N.; Zhang, Q.H.; Wang, Q.; Luo, L.; Wang, X.C.C.; Xiong, J.Q.; Han, J.X. Current status and characteristics of urban landscape lakes in China. *Sci. Total Environ.* **2020**, *712*, 135669. [CrossRef]
8. Ao, D.; Luo, L.; Dzakpase, M.; Chen, R.; Xue, T.; Wang, X.C.C. Replenishment of landscape water with reclaimed water: Optimization of supply scheme using transparency as an indicator. *Ecol. Indic.* **2018**, *88*, 503–511. [CrossRef]
9. Hu, S.J.; Niu, Z.G.; Chen, Y.F.; Li, L.F.; Zhang, H.Y. Global wetlands: Potential distribution, wetland loss, and status. *Sci. Total Environ.* **2017**, *586*, 319–327. [CrossRef]
10. Yuan, D.; Meng, X.; Duan, C.; Wei, Z.; Gao, W.; Chang, J.; Lv, X.; Pan, Y. Effects of water exchange rate on morphological and physiological characteristics of two submerged macrophytes from Erhai Lake. *Ecol. Evol.* **2018**, *8*, 12750–12760. [CrossRef]
11. Wu, B.B.; Wang, G.Q.; Wang, Z.W.; Liu, C.M.; Ma, J.M. Integrated hydrologic and hydrodynamic modeling to assess water exchange in a data-scarce reservoir. *J. Hydrol.* **2017**, *555*, 15–30. [CrossRef]
12. Gao, Q.F.; He, G.J.; Fang, H.W.; Bai, S.; Huang, L. Numerical simulation of water age and its potential effects on the water quality in Xiangxi Bay of Three Gorges Reservoir. *J. Hydrol.* **2018**, *566*, 484–499. [CrossRef]
13. Pilotti, M.; Simoncelli, S.; Valerio, G. A simple approach to the evaluation of the actual water renewal time of natural stratified lakes. *Water Resour. Res.* **2014**, *50*, 2830–2849. [CrossRef]
14. Huang, L.; Fang, H.W.; He, G.J.; Jiang, H.L.; Wang, C.H. Effects of internal loading on phosphorus distribution in the Taihu Lake driven by wind waves and lake currents. *Environ. Pollut.* **2016**, *219*, 760–773. [CrossRef]
15. Huang, A.P.; Liu, X.B.; Peng, W.Q.; Dong, F.; Wang, W.J. Spatiotemporal Characteristics of Water Age in the Largest Freshwater Lake in China. In *World Environmental and Water Resources Congress 2019: Hydraulics, Waterways, and Water Distribution System Analysis*; American Society of Civil Engineers: Pittsburgh, PA, USA, 2019; pp. 376–381.
16. Amorim, L.F.; Martins, J.R.S.; Nogueira, F.F.; Silva, F.P.; Duarte, B.P.S.; Magalhaes, A.A.B.; Vincon-Leite, B. Hydrodynamic and ecological 3D modeling in tropical lakes. *SN Appl. Sci.* **2021**, *3*, 444. [CrossRef]
17. Peng, F.J.; Li, K.F.; Liang, R.F.; Li, X.T.; Zhang, P.; Yuan, Q.; Ji, Q.F.; Zhu, Z.X.; Wang, Y.M. Shallow lake water exchange process before and after water diversion projects as affected by wind field. *J. Hydrol.* **2021**, *592*, 125785. [CrossRef]
18. Li, Y.P.; Archarya, K.; Yu, Z.B. Modeling impacts of Yangtze River water transfer on water ages in Lake Taihu, China. *Ecol. Eng.* **2011**, *37*, 325–334. [CrossRef]
19. Djihouessi, M.B.; Aina, M.P. A review of hydrodynamics and water quality of Lake Nokoué: Current state of knowledge and prospects for further research. *Reg. Stud. Mar. Sci.* **2018**, *18*, 57–67. [CrossRef]

20. Li, Y.P.; Tang, C.Y.; Zhu, J.T.; Pan, B.Z.; Anim, D.O.; Ji, Y.; Yu, Z.B.; Acharya, K. Parametric uncertainty and sensitivity analysis of hydrodynamic processes for a large shallow freshwater lake. *Hydrol. Sci. J.* **2015**, *60*, 1078–1095. [CrossRef]
21. Huang, M.T.; Tian, Y. An Integrated Graphic Modeling System for Three-Dimensional Hydrodynamic and Water Quality Simulation in Lakes. *Int. J. Geo-Inf.* **2019**, *8*, 18. [CrossRef]
22. You, X.Y.; Zhang, C.X. On improvement of water quality of a reservoir by optimizing water exchange. *Environ. Prog. Sustain.* **2017**, *37*, 399–409. [CrossRef]
23. Luyiga, S.; Haande, S.; Semyalo, R.P.; Kizito, Y.S.; Miyingo-Kezimbira, A.; Brettum, P.; Solheim, A.L.; Odong, R.; Asio, S.M.; Jensen, K.H.; et al. How water exchange and seasonality affect the eutrophication of Murchison Bay, Lake Victoria. *Limnologica* **2015**, *53*, 60–73. [CrossRef]
24. Zhu, W.; Wan, L.; Zhao, L.F. Effect of nutrient level on phytoplankton community structure in different water bodies. *J. Environ. Sci.* **2010**, *22*, 32–39. [CrossRef]
25. Wu, Y.; Dai, R.; Xu, Y.F.; Han, J.G.; Li, P.P. Statistical assessment of water quality issues in Hongze Lake, China, related to the operation of a water diversion project. *Sustainability* **2018**, *10*, 1885. [CrossRef]
26. Zhang, R.Y.; Wu, B.S. Environmental Impacts of High Water Turbidity of the Niulan River to Dianchi Lake Water Diversion Project. *J. Environ. Eng.* **2020**, *146*, 05019006. [CrossRef]
27. Min, P.; Song, W.W.; Zhang, P.; Shao, Y.X.; Li, L.; Pang, Y.; Wang, J.J.; Xu, Q. Research into the Eutrophication of an Artificial Playground Lake near the Yangtze River. *Sustainability* **2018**, *10*, 867. [CrossRef]
28. Fomarelli, R.; Galelli, S.; Castelletti, A.; Antenucci, J.P.; Marti, C.L. An empirical modeling approach to predict and understand phytoplankton dynamics in a reservoir affected by interbasin water transfers. *Water Resour. Res.* **2013**, *49*, 3626–3641. [CrossRef]
29. Gohari, A.; Eslamian, S.; Mirchi, A.; Abedi-Koupaei, J.; Bavani, A.M.; Madani, K. Water transfer as a solution to water shortage: A fix that can Backfire. *J. Hydrol.* **2013**, *491*, 23–39. [CrossRef]
30. Tang, C.H.; Yi, Y.J.; Yang, Z.F.; Sun, J. Risk forecasting of pollution accidents based on an integrated Bayesian Network and water quality model for the South to North Water Transfer Project. *Ecol. Eng.* **2016**, *96*, 109–116. [CrossRef]
31. Tang, C.Y.; He, C.; Li, Y.P.; Acharya, K. Diverse responses of hydrodynamics, nutrients and algal biomass to water diversion in a eutrophic shallow lake. *J. Hydrol.* **2021**, *593*, 125933. [CrossRef]
32. Gao, X.P.; Xu, L.P.; Zhang, C. Estimating renewal timescales with residence time and connectivity in an urban man-made lake in China. *Environ. Sci. Pollut. Res. Int.* **2016**, *23*, 13973–13983. [CrossRef] [PubMed]
33. Zhang, M.M.; Wang, S.; Fu, B.J.; Gao, G.Y.; Shen, Q. Ecological effects and potential risks of the water diversion project in the Heihe River Basin. *Sci. Total Environ.* **2018**, *619–620*, 794–803. [CrossRef] [PubMed]
34. Kang, M.X.; Tian, Y.M.; Zhang, H.Y.; Wang, D.H. Relationship between Hydrodynamic Conditions and Water Quality in Landscape Water Body. *IOP Conf. Ser. Earth Environ. Sci.* **2018**, *112*, 012001. [CrossRef]
35. Li, D.F.; He, W.X.; Lin, B.; Bai, F.Q.; Xie, F. Study and Analysis on Strengthening Hydrodynamic of Guazhuhu Lake Based on 2D-Numerical Simulation. In Proceedings of the 2017 6th International Conference on Energy and Environmental Protection (ICEEP 2017), Zhuhai, China, 29–30 June 2017. [CrossRef]
36. Yan, L.I.; Guan, H.L.; Wang, Y. Effect of water diversion from the Yangtze River to Chang Lake on hydrodynamic characteristics and water quality of Chang Lake. *IOP Conf. Ser. Earth Environ. Sci.* **2018**, *153*, 062060. [CrossRef]
37. Huang, J.C.; Yan, R.H.; Gao, J.F.; Zhang, Z.M.; Qi, L.Y. Modeling the impacts of water transfer on water transport pattern in Lake Chao, China. *Ecol. Eng.* **2016**, *95*, 271–279. [CrossRef]
38. Dai, C.; Tan, Q.; Lu, W.T.; Liu, Y.; Guo, H.C. Identification of optimal water transfer schemes for restoration of a eutrophic lake: An integrated simulation-optimization method. *Ecol. Eng.* **2016**, *95*, 409–421. [CrossRef]
39. Li, Y.P.; Tang, C.Y.; Wang, C.; Tian, W.; Pan, B.Z.; Hua, L.; Lau, J.; Yu, Z.B.; Archarya, K. Assessing and modeling impacts of different inter-basin water transfer routes on Lake Taihu and the Yangtze River, China. *Ecol. Eng.* **2013**, *60*, 399–413. [CrossRef]
40. Xu, R.C.; Pang, Y.; Hu, Z.B.; Kaisam, J.P. Dual-Source Optimization of the "Diverting Water from the Yangtze River to Tai Lake (DWYRTL)" Project Based on the Euler Method. *Complexity* **2020**, *2020*, 3256596. [CrossRef]
41. Song, W.W.; Xu, Q.; Fu, X.Q.; Zhang, P.; Pang, Y.; Song, D.H. Research on the Relationship between Water Diversion and Water Quality of Xuanwu Lake, China. *Int. J. Environ. Res. Public Health* **2018**, *15*, 1262. [CrossRef]
42. You, A.J.; Hua, L. Optimization and Effect of Inner Water Diversion and Distribution in the West Lake of Hangzhou. *IOP Conf. Ser. Earth Environ. Sci.* **2019**, *264*, 012018. [CrossRef]
43. Song, W.W.; Fu, X.Q.; Pang, Y.; Song, D.H.; Xu, Q.; Zhang, P. Research on Water Environment Regulation of Artificial Playground Lake Interconnected Yangtze River. *Int. J. Environ. Res. Public Health* **2018**, *15*, 2110. [CrossRef] [PubMed]
44. Zhang, M.X.; Dolatshah, A.; Zhu, W.L.; Yu, G.L. Case Study on Water Quality Improvement in Xihu Lake through Diversion and Water Distribution. *Water* **2018**, *10*, 333. [CrossRef]
45. Jensen, B.; Carstensen, S.; Christensen, E.D. Mixing of stratified flow around bridge piers in steady current. *J. Hydraul. Eng.* **2018**, *144*, 04018041. [CrossRef]
46. Leli, I.T.; Stevaux, J.C. Lake-islands: A distinct morphology of river systems. *J. S. Am. Earth Sci.* **2021**, *111*, 103424. [CrossRef]
47. Pandey, M.; Sharma, P.K.; Ahmad, Z.; Singh, U.K.; Karna, N. Three Dimensional Velocity Measurements around Bridge Piers in Gravel Bed. *Mar. Georesour. Geotechnol.* **2017**, *36*, 663–676. [CrossRef]
48. Gautam, P.; Eldho, T.I.; Mazumder, B.S.; Behera, M.R. Experimental Study of Flow and Turbulence characteristics around Simple and Complex Piers using PIV. *Exp. Therm. Fluid Sci.* **2018**, *100*, 193–206. [CrossRef]

49. Namaee, M.R.; Sui, J. Velocity profiles and turbulence intensities around side-by-side bridge piers under ice-covered flow condition. *J. Hydrol. Hydromech.* **2020**, *68*, 70–82. [CrossRef]
50. Izadinia, E.; Heidarpour, M.; Schleiss, A.J. Investigation of turbulence flow and sediment entrainment around a bridge pier. *Stoch. Environ. Res. Risk Asses.* **2013**, *27*, 1303–1314. [CrossRef]
51. Guo, X.F.; Chen, C.H.; Tang, J.J. Numerical simulation of the hydrodynamic effects of an artificial island. *Fresenius Environ. Bull.* **2018**, *27*, 2671–2682.
52. Yan, H.K.; Wang, N.; Yu, T.L.; Song, N.Q. Hydrodynamic behavior and the effects of water pollution from Dalian's large-scale offshore airport island in Jinzhou Bay, China. *J. Waterw. Port Coast. Ocean Eng.* **2015**, *141*, 05014003. [CrossRef]
53. Liu, T.; Liu, Y.H.; Hou, Z.Q. Numerical Study on Influence of Water Exchange for Artificial Island Group. *IOP Conf. Ser. Earth Environ. Sci.* **2018**, *171*, 012016. [CrossRef]
54. Branson, P.M.; Ghisalberti, M.; Ivey, G.N. Three-dimensionality of shallow island wakes. *Environ. Fluid Mech.* **2019**, *19*, 1393–1416. [CrossRef]
55. Carnacina, I.; Leonardi, N.; Pagliara, S. Characteristics of Flow Structure around Cylindrical Bridge Piers in Pressure-Flow Conditions. *Water* **2019**, *11*, 2240. [CrossRef]
56. Hou, L.; Wang, J.X.; Liang, Y. Study on the application of distortion similarity theory to fishway model test. *Eng. J. Wuhan Unv.* **2021**, *54*, 298–306. [CrossRef]
57. Zhang, B.M. Distorted scale model and scale effects. In Proceedings of the International Symposium on Hydraulic Research in Nature and Laboratory Proceedings, Wuhan, China, 17–20 November 1992; pp. 7–10.
58. Bansal, M.K. Dispersion in Natural Streams. *J. Hydraul. Div.* **1971**, *97*, 1867–1886. [CrossRef]
59. Rulli, M.C.; Rosso, R. Modeling catchment erosion after wildfires in the San Gabriel Mountains of southern California. *Geophys. Res. Lett.* **2005**, *32*, 312–321. [CrossRef]
60. Seo, H.; Kim, K.C. Experimental study on flow and turbulence characteristics of bubbly jet with low void fraction. *Int. J. Multiph. Flow* **2021**, *142*, 103738. [CrossRef]
61. Yang, P.; Zhang, H.; Wang, Y.; Wang, Y.; Wang, Y. Overland flow velocities measured using a high-resolution particle image velocimetry system. *J. Hydrol.* **2020**, *590*, 125225. [CrossRef]
62. Liu, D.M.; Ma, L.B.; Li, N.; Zhao, Y.Z.; Cheng, H. Experimental research on flow field of high head pump turbine based on PIV test. *IOP Conf. Ser. Earth Environ. Sci.* **2021**, *627*, 012016. [CrossRef]
63. Bai, R.N.; Zhu, D.J.; Chen, H.; Li, D.X. Laboratory Study of Secondary Flow in an Open Channel Bend by Using PIV. *Water* **2019**, *11*, 659. [CrossRef]
64. Xiong, J.L.; Shen, J.; Qin, Q.B.; Du, J.B. Water exchange and its relationships with external forcings and residence time in Chesapeake Bay. *J. Mar. Syst.* **2020**, *215*, 103497. [CrossRef]
65. Qi, H.D.; Lu, J.Z.; Chen, X.L.; Sauvage, S.; Sanchez-Perez, J.M. Water age prediction and its potential impacts on water quality using a hydrodynamic model for Poyang Lake, China. *Environ. Sci. Pollut. Res.* **2016**, *23*, 13327–13341. [CrossRef] [PubMed]
66. Gao, X.P.; Xu, L.P.; Zhang, C. Modelling the effect of water diversion projects on renewal capacity in an urban artificial lake in China. *J. Hydroinform.* **2015**, *17*, 990–1002. [CrossRef]
67. Jiang, X.H.; Liu, C.M. Water renewal time of the Yellow River mainstream based on reservoir action. *J. Geogr. Sci.* **2013**, *23*, 113–122. [CrossRef]
68. Hua, Z.L.; Gu, L.; Liu, X.D. Improving water exchange rate of shallow lakes through water diversion works. *Water Resour. Protect.* **2009**, *25*, 9–17. (In Chinese)
69. Yao, Y.M.; Peng, H.; Du, Y.J.; Liu, L. Numerical Study on water exchange in Xiangshangang Bay. *Acta Ocean. Sin.* **2014**, *36*, 126–130. (In Chinese) [CrossRef]
70. Zhang, W.X. Study on Hydrodynamic and Water Exchange Characteristics of Caofeidian Wetland. *Shijiazhuang Tiedao Univ.* **2019**. (In Chinese) [CrossRef]
71. Zhang, Y.M.; Zhang, Y.C.; Zhang, L.J.; Gao, Y.X.; Zhao, Y. The influence of lake hydrodynamics on blue algal growth. *China Environ. Sci.* **2007**, *27*, 707–711. (In Chinese)
72. Mitrovic, S.M.; Hardwick, L.; Dorani, F. Use of flow management to mitigate cyanobacterial blooms in the Lower Darling River, Australia. *J. Plankton Res.* **2011**, *33*, 229–241. [CrossRef]
73. Yan, B.L.; Lin, H.J. Research on Diversion Water Scheme of Improving Environmental Water Quality in the Hangjiahu Area. *China Rural. Water Hydropower* **2008**, *9*, 33–35. (In Chinese)
74. Yan, Y.X.; Jiang, X.X.; Ruan, X.H.; Li, Y.; Zhao, Z.H.; Ni, L.X.; Zhang, Y. Water pollution characteristics and control measures in cities of plain river network area. *Water Resour. Prot.* **2008**, *25*, 1–3. (In Chinese)
75. Engelmann, L.; Ihme, M.; Wlokas, I.; Kempf, A. Towards the Suitability of Information Entropy as an LES Quality Indicator. *Flow Turbul. Combust.* **2021**, *108*, 353–385. [CrossRef]
76. Engelmann, L.; Wlokas, I.; Kempf, A.M. What can we learn from information-entropy about turbulence and Large-Eddy-Simulation? *PAMM* **2019**, *19*, e201900253. [CrossRef]
77. Yan, Y.; Wang, J. Information Entropy Embedded Back Propagation Neural Network Approach for Debris Flows Hazard Assessment. *IOP Conf. Ser. Earth Environ. Sci.* **2020**, *453*, 012015. [CrossRef]
78. Akundi, A.; Smith, E.; Tseng, T.L. Information entropy applied to software based control flow graphs. *Int. J. Syst. Assur. Eng. Manag.* **2018**, *9*, 1080–1091. [CrossRef]

79. Shannon, C.E.; Weaver, W.; Burks, A.W. *The Mathematical Theory of Communication*; Wiley: New York, NY, USA, 1951.
80. Murtaza, G.; Hashmi, H.M.; Naeem, U.A.; Khan, D.; Ahmad, N. Effect of bridge pier shape on scour depth at uniform single bridge pier. *Mehran Univ. Res. J. Eng. Technol.* **2018**, *37*, 539–544. [CrossRef]
81. Zhang, X.Q.; Wang, T.; Lu, X.B. Influence of bridge piers shapes on the flow of the lower Yellow River. *Water Pract. Technol.* **2021**, *16*, 661–680. [CrossRef]